

CHAPTER VII

Isotopic substitution of a hydrogen bond: a near IR study of the intramolecular states in $(DF)_2$

7.1 Introduction

The dynamics of small hydrogen bonded clusters continues to be a focus of increasing research effort, due to a mixture of experimental accessibility, theoretical tractability and the intriguing repertoire of dynamical behavior these complexes can display. As one celebrated example taken from the high resolution near-IR literature, the time scale for energy flow from the high frequency (*intramolecular*) vibrations into the low frequency (*intermolecular*) modes can be surprisingly slow,¹ resulting in predissociation lifetimes 10^5 - 10^6 fold longer than the internal vibrational “clock” for oscillation of the covalent bonds. In addition, these unimolecular energy flow rates are quite sensitive to the specific mode excited,²⁻⁴ demonstrating a highly *non-statistical* dependence on internal energy.⁵ Furthermore, the presence of light H atoms in the cluster typically results in large amplitude, highly anharmonic motion of the molecular subunits. For systems with sufficient molecular symmetry, such large amplitude motion may result in quantum mechanical tunneling between equivalent configurations⁶⁻⁸ which can be observed at high resolution via tunneling splittings. This range of quantum state

resolved behavior provides numerous spectroscopic opportunities for probing detailed dynamics on the associated inter- and intramolecular potentials, and thereby rigorously testing state-of-the-art *ab initio* and semiempirical energy surfaces for hydrogen bonding.

As the simplest 4-atom prototype of a hydrogen bonded cluster, the hydrogen fluoride dimer (HF)₂ has arguably become the “benchmark” system for experimental and theoretical studies of hydrogen bonding. The hydrogen fluoride dimer and its (DF)₂ isotopomer were first observed with state resolved methods more than two decades ago by Dyke et al.⁹ This pioneering work employed radiofrequency and microwave spectroscopy to characterize the vibrationally averaged dimer “geometry” and tunneling splittings of the energy levels. In a series of subsequent microwave measurements, the tunneling splitting and rotational energy progressions were mapped out for both isotopes in a range of *K* manifolds.¹⁰⁻¹² Later, Pine et. al⁴ observed rotationally resolved structure for (HF)₂ in the near IR, corresponding to high frequency intramolecular excitation of both ν_1 , “free” HF, and ν_2 , “bound” HF stretching modes. The presence of sharp rotational structure indicated the lifetimes for these vibrationally metastable states to be considerably longer than previously anticipated,¹³ thus establishing the feasibility of studying hydrogen bonded clusters with high resolution techniques in the near-IR.

Subsequent high resolution studies by Pine and coworkers¹⁴⁻¹⁶ in equilibrium cooled cells determined the *K* dependent vibrational origins for both ν_1 and ν_2 intramolecular fundamentals in both HF and DF dimers. With the

additional tools of optothermal and photofragment translational spectroscopies,¹⁷⁻¹⁹ HF dimer has continued to be investigated with considerable diligence, yielding accurate dissociation energies,¹⁷ product state distributions,^{17,18} and predissociation lifetimes.¹⁹ As mentioned above, these high resolution IR laser studies have revealed mode specific predissociation behavior; specifically, states with one quanta of “bound” HF stretch excitation are observed to predissociate a factor of 30-50 times more rapidly than the corresponding excitation of the “free” HF stretch at *higher* energy. Additional studies on overtone excitation of the intramolecular states in HF dimer²⁰⁻²² have yielded further information on tunneling splittings, predissociation rates, and the “bound” vs. “free” HF stretch character in these vibrational polyad levels. These experimental efforts have been paralleled by advances in the development both of *ab initio*/semiempirical potential energy surfaces,²³⁻³¹ as well as the theoretical tools for analysis and interpretation of the large amplitude quantum vibrational motion in full (i.e., 6-D) dimensionality.³²⁻³⁶

As a result of significant zero point effects for such light species and weakly bonded potentials, there has been a keen interest in obtaining the corresponding high resolution spectroscopic information on DF dimer. Despite this interest, there has been a surprisingly limited amount of high resolution IR spectral information available in the literature. For example, rotational constants have been reported for HF dimer intramolecular states,^{4,14} but not for the corresponding DF dimer. Similarly, detailed studies of vibrational predissociation have been performed for the intramolecular states of HF dimer,^{3,4,19,37} whereas the

rates for DF dimer have not been available. Sophisticated theoretical efforts have been used to predict intramolecular excited energies,³⁶ tunneling splittings,³⁸ and vibrational predissociation rates for HF dimer,^{36,39-41} but relatively little is known about DF dimer. The present study is directed toward filling this clear gap in high resolution spectral information on DF dimer.

The relative paucity of high resolution near IR data on DF dimer has been largely due to experimental constraints. The intramolecular stretching frequencies in DF dimer occur slightly red shifted from the 2906 cm^{-1} DF $\nu=1\leftarrow 0$ fundamental. This is near the limit of the operational range of cw single mode color center lasers, and thus restricting the application of optothermal spectroscopic methods. Indeed, prior to this work, the only previous near-IR experimental measurements on DF dimer were from Pine et. al.,¹⁴ based on difference frequency laser and direct absorption techniques in an equilibrium cooled cell at $\approx 215\text{ K}$. However, in these previous studies the combination of spectral congestion and finite pressure/Doppler broadening under such relatively “high temperature” cooled cell conditions limited the high resolution spectral analysis. In the current study, difficulties due to thermal congestion and IR wavelength coverage are circumvented by a combination of i) direct absorption spectroscopy in a supersonic cooled, slit jet expansion cluster source at $\leq 10\text{ K}$, and ii) difference frequency laser techniques to achieve high resolution access to the 2900 cm^{-1} DF dimer fundamental region. The net result is uncongested jet-cooled spectroscopy of $(\text{DF})_2$, with sub-Doppler instrumental resolution capable

of detecting the slight rovibrational line broadening due to slow vibrational predissociation.

7.2 Experiment

The experimental technique employed is essentially identical to that used for previous studies,^{42,43} with minor modifications for maximum generation of (DF)₂ clusters. The spectra of the ν_1 and ν_2 (DF)₂ intramolecular fundamentals are recorded using the combination of a slit supersonic jet for cluster formation and direct absorption IR methods based on a tunable difference frequency laser spectrometer, as described in detail in Chapter 2. The (DF)₂ is produced in the slit expansion with typical backing pressures of 500 Torr (1 Torr = 133.322 Pa) of 0.6% DF in a 50%/35%/15% mix of Ar, Ne and He, resulting in rotational temperatures of 8-10 K. The relative infrared frequencies are determined by monitoring dye laser transmission fringes through a stabilized Fabry-Perot optical transfer cavity,^{42,43} to which the Ar⁺ laser is servo loop locked as well. This technique permits measurement of *relative* frequencies to better than 0.0001 cm⁻¹, as verified by routine agreement with microwave ground state combination differences at the 1-2 MHz level. *Absolute* frequencies are determined by reference to DF monomer lines P(1) and P(3) in the slit jet at 2884.94325 cm⁻¹ and 2839.78537 cm⁻¹, respectively.⁴⁵ This procedure allows the transition frequencies and vibrational origins to be reported to an accuracy of 0.0002 cm⁻¹.

7.3 Results and analysis

7.3.1 Background

Consistent with the previously established convention,^{4,12} the rotational progressions for each vibration-tunneling band observed are fit to a standard polynomial expansion in $J(J+1)$ for a slightly asymmetric prolate top ($K = K_a$):

$$E_K(J) = v_K + \left[\overline{B}_K \pm \frac{1}{4} b_K \mathbf{d}_{K1} \right] J(J+1) - \left[D_K \pm \frac{1}{2} d_K \mathbf{d}_{K1} \right] J^2(J+1)^2 + H_K J^3(J+1)^3 \quad (7.1)$$

In Eq. (7.1) v_K is defined as the energy of the $J = 0$ (extrapolated for $K > 0$) state for a given K level. Furthermore, $\overline{B}_K = (B_K + C_K) / 2$, D_K and H_K are K -dependent rotational and distortion constants, while the Kronecker delta \mathbf{d}_{K1} brings in asymmetry splittings which are significant only for $K = 1$ levels. For all the spectra presented in this chapter, the J and tunneling state labeling is unambiguously confirmed by ground state combination differences generated from previous microwave¹² studies and to which the ground state constants are fixed in the least squares fits. The sextic centrifugal distortion constant H_K is set to zero in the upper state due to insufficient number of high J states populated in the 8-10 K supersonic jet.

The *magnitude* of the tunneling splitting for each vibration and K state is defined as the difference in the vibrational term values (v_K) for the two tunneling

states, which is readily determined from the spectroscopic fits to Eq. (7.1). The *sign* of the tunneling splitting, on the other hand, rigorously requires assignment of the tunneling symmetry (Γ_{tun}) to either A^+ (symmetric) or B^+ (anti-symmetric) within a given tunneling pair. If Γ_{tun} is a meaningful symmetry label, the $\Gamma_{\text{tun}} = B^+$ state has an additional node along the tunneling coordinate, and is therefore anticipated to be higher in energy than the $\Gamma_{\text{tun}} = A^+$ state. This leads to the signed definition²² of tunneling splitting as follows:

$$\Delta\nu_{\text{tun}} = \nu_K(\Gamma_{\text{tun}} = B^+) - \nu_K(\Gamma_{\text{tun}} = A^+) \quad (7.2)$$

As discussed in the previous chapter and elsewhere,⁴⁶ only the product $\Gamma_{\text{vib-tun}} = \Gamma_{\text{vib}} \otimes \Gamma_{\text{tun}}$ can be inferred directly from the spectra. The vibrational symmetries of the ν_1 and ν_2 intramolecular modes, however, have been assigned by Mills⁴⁷ to $\Gamma_{\text{intra}} = B^+$ and A^+ , respectively. This permits determination of Γ_{tun} in the excited state and therefore the tunneling splitting as a signed quantity. Such an assignment first requires factoring the total vibrational-rotational-tunneling symmetry (Γ_{VRT}) into vibrational (Γ_{vib}), rotational (Γ_{rot}) and tunneling (Γ_{tun}) components. This factoring may not be meaningful if unimolecular state mixing of these zeroth order levels is sufficiently large, which could in principle invert the ordering of tunneling levels. However, from systematic studies of fundamental and combination band spectroscopy in our laboratory,^{46,48,49} this appears not to be the case in both HF and DF dimer for single quantum HF/DF

stretch excitation. Specifically, all of the tunneling splittings reported in the present study are found to be positive, i.e., the upper/lower tunneling levels are consistent with $\Gamma_{\text{tun}} = B^+/A^+$, respectively.

7.3.2 ν_1 (“free” DF stretch) : $K = 0 \rightarrow 0$

The ν_1 stretching mode (“free” DF stretch) is expected to be a hybrid band, i.e., supporting both perpendicular ($\Delta K = \pm 1$) and parallel ($\Delta K = 0$) transitions. However, for a ν_1 transition dipole moment aligned along the free DF monomer axis one would predict parallel transitions to be approximately four times weaker than the corresponding perpendicular transitions, due to a strongly “bent” equilibrium geometry.³¹ Consistent with this prediction, both $K = 1 \leftarrow 0$ and $K = 0 \leftarrow 0$ subbands of the ν_1 mode in (HF)₂ were observed by Pine et al. with a 5:1 intensity ratio.^{14,19} For the corresponding (DF)₂ ν_1 mode, on the other hand, Pine et. al. only reported the two $K = 1 \leftarrow 0$ (2897.8 cm⁻¹) and the $K = 0 \leftarrow 1$ (2866.4 cm⁻¹) perpendicular subbands. This suggests that the strong propensity for perpendicular vs. parallel excitation for ν_1 in (HF)₂ holds also for (DF)₂, although the lack of parallel subbands prohibits both quantifying this propensity and the determination of K spacings (or alternatively, an effective A constant) in either the ground or vibrationally excited states.

The $K = 0 \leftarrow 0$ subband of the ν_1 mode of $(DF)_2$ should absorb at roughly one A constant below the $K = 1 \leftarrow 0$ subband, which guides our spectral search. For the ν_1 mode of $(HF)_2$, A is known¹⁴ to be $\approx 32 \text{ cm}^{-1}$. Since the A rotational

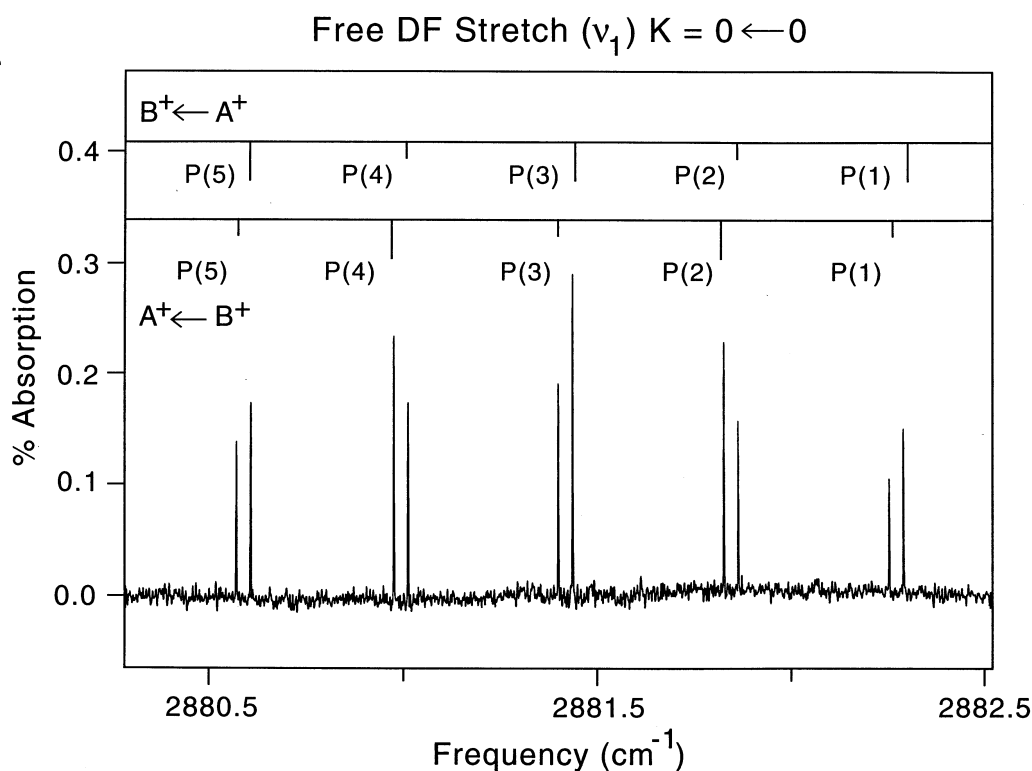


Figure 7.1 A section of the spectrum of the $K = 0 \leftarrow 0$ subband of the ν_1 intramolecular mode ($T_{\text{rot}} = 10 \pm 2 \text{ K}$) of $(DF)_2$. The A^+ and B^+ symmetry labels refer to $\Gamma_{\text{vib-tun}}$, the vibration-tunneling symmetry. Note the 7:5 J -dependent intensity alternation in both tunneling bands due to nuclear spin statistics, as well as the considerably narrower predissociation linewidths than observed in $(DF)_2$.

constant is inversely proportional to the moment of inertia about the dimer intermolecular axis (which essentially intersects the two fluorine atoms), deuterium substitution should *decrease* A by a factor of ≈ 2 ; this predicts a corresponding ν_1 parallel $K = 0 \leftarrow 0$ subband approximately 16 cm^{-1} to the red. Consistent with this prediction, the ν_1 parallel $K = 0 \leftarrow 0$ subband is observed with an origin almost 15 cm^{-1} redshifted from the perpendicular $K = 1 \leftarrow 0$ subband origin. Shown in Figure 7.1 is a section of the P branch that clearly demonstrates a near symmetric top like spectrum, the presence of tunneling pairs of subbands, and the even:odd J intensity alternation associated with identical DF monomer subunits. This intensity alternation, arising from $I_D = 1$ and $I_F = 1/2$ nuclear spin statistics, is 5:7 for even:odd J with transitions originating from the symmetric (A^+) tunneling level and 7:5 for even:odd J with transitions originating from the antisymmetric (B^+) tunneling level.⁵⁰ This alternation allows unambiguous assignment of the ground state tunneling symmetry, which is further verified via ground state combination differences. All of the observed transitions are reported in Table 7.1. The rotational progressions for each tunneling level are fit to Eq. (7.1) for the $\Gamma_{\text{vib-tun}} = B^+ \leftarrow A^+$ and $\Gamma_{\text{vib-tun}} = A^+ \leftarrow B^+$ bands, respectively; the results are summarized in Table 7.2. The residual standard deviations for both fits are less than 0.0002 cm^{-1} i.e., no signs of rotational perturbations are observed. The tunneling splitting for the $K = 0, \nu_1$ level, as defined by Eq. (2), is $0.01668(14)$

cm^{-1} , where the uncertainty reflects 2σ differences in the two tunneling origins.

From suitable differences in the $K = 1 \leftarrow 0$ and $0 \leftarrow 1$ vibrational origins of Pine et.

Table 7.1 The observed and fitted transition frequencies for ν_1 “free DF stretch”. The numbers in parentheses represent the deviations (obs – calc) from the least-squares fit of each VRT band in units of the last reported digit. The absolute frequencies are determined by reference to P(1) of DF monomer at 2884.94325^{a} cm^{-1} , with an accuracy of 0.0002 cm^{-1} .

$\Gamma_{\text{vib-tun}}$	$\nu_1 \ K = 0 \leftarrow 0$		$\nu_1 \ K = 1 \leftarrow 0$	
	$\text{B}^+ \leftarrow \text{A}^+$	$\text{A}^+ \leftarrow \text{B}^+$	$\text{B}^+ \leftarrow \text{A}^+$	$\text{A}^+ \leftarrow \text{B}^+$
R(9)	2886.9581(0)	2886.9233(2)	2901.98849(-4)	2901.95887(-4)
R(8)	2886.5249(1)	2886.4898(2)	2901.56927(-6)	2901.53943(-7)
R(7)	2886.0931(1)	2886.0578(0)	2901.15021(-4)	2901.12018(-3)
R(6)	2885.6627(0)	2885.6273(2)	2900.73131(4)	2900.70100(-6)
R(5)	2885.2340(2)	2885.1983(2)	2900.31240(4)	2900.28203(-3)
R(4)	2884.8066(1)	2884.7708(1)	2899.89373(-3)	2899.86319(-4)
R(3)	2884.3807(0)	2884.3429(0)	2899.47523(-3)	2899.44471(9)
R(2)	2883.9566(0)	2883.9208(1)	2899.05694(-2)	2899.02626(3)
R(1)	2883.5343(1)	2883.4982(0)	2898.63889(0)	2898.60813(1)
R(0)	2883.1136(0)	2883.0776(1)	2898.22111(0)	2898.19029(-2)
P(1)	2882.2775(0)	2882.2415(0)		
P(2)	2881.8622(0)	2881.8262(-1)	2896.96979(0)	2896.93907(-5)
P(3)	2881.4488(0)	2881.4131(0)	2896.55365(4)	2896.52296(1)
P(4)	2881.0374(0)	2881.0017(-1)	2896.13780(5)	2896.10728(-4)
P(5)	2880.6280(0)	2880.5925(0)	2895.72256(2)	2895.69229(0)
P(6)	2880.2206(-1)	2880.1854(0)	2895.30796(0)	2895.27782(-7)
P(7)	2879.8153(-1)	2879.7802(-1)	2894.89407(2)	2894.86431(8)
P(8)	2879.4122(-1)	2879.3773(-1)	2894.48096(4)	2894.45137(4)
P(9)	2879.0113(-1)	2878.9766(-2)	2894.06870(9)	2894.03932(3)
P(10)		2878.5781(-2)	2893.65730(9)	2893.62818(2)
P(11)		2878.1821(-1)	2893.24674(-6)	2893.21805(0)
P(12)			2892.83740(-7)	2892.80916(2)
P(13)			2892.42941(8)	2892.40106(-7)
Q(1)			2897.80873(2)	2897.77790(-5)
Q(2)			2897.81887(0)	2897.78817(2)
Q(3)			2897.83414(3)	2897.80353(7)
Q(4)			2897.85438(-4)	2897.82389(2)
Q(5)			b	2897.84939(0)
Q(6)			2897.91023(-5)	c
Q(7)			2897.94581(-3)	2897.91573(0)
Q(8)			2897.98643(-4)	2898.95659(2)
Q(9)			2898.03220(1)	2898.00248(-2)
Q(10)			2898.08298(-2)	2898.05358(2)
Q(11)			2898.13888(-2)	2898.10970(-2)
Q(12)			2898.19993(4)	d
Q(13)			2898.26602(3)	2898.23736(-4)
Q(14)			2898.33734(13)	2898.30897(4)
Q(15)			2898.41343(-12)	

a. Reference 45

- b. overlapped with Q(6) of $\nu_1 A^+ \leftarrow B^+$
- c. overlapped with Q(5) of $\nu_1 B^+ \leftarrow A^+$
- d. overlapped with R(0) of ArDF

Table 7.2 Molecular constants (cm^{-1}) determined from fits of the transition frequencies to Eq. (7.1) for ν_1 “free DF stretch” bands. The uncertainties in parentheses represent 2σ , from the least squares fit, in the units of the last reported digit.

$\Gamma_{\text{vib-tun}}=$	$\nu_1 K = 0 \leftarrow 0$		$\nu_1 K = 1 \leftarrow 0$	
	$B^+ \leftarrow A^+$	$A^+ \leftarrow B^+$	$B^+ \leftarrow A^+$	$A^+ \leftarrow B^+$
n_0	2882.69456(8)	2882.65852(11)	2897.80363(4)	2897.77284(4)
\bar{B}'_K	0.209467(4)	0.209463(6)	0.2099232(12)	0.2099160(12)
$b'_K/10^{-3}$	----	----	4.72(2)	4.72(4)
$D'_K/10^{-6}$	1.904(40)	1.937(51)	1.859(6)	1.854(8)
$d'_K/10^{-6}$	----	----	0.152(12)	0.131(12)
σ_{rms}	0.00008	0.00012	0.00005	0.00005

al.,¹⁴ the $K = 0$, ν_1 tunneling splitting had been previously reported to be $0.01630(70) \text{ cm}^{-1}$, i.e., with corresponding 2σ error limits consistent with the present measurement.

7.3.3 ν_1 (“free” DF stretch): $K = 1 \rightarrow 0$

As stated earlier, the ν_1 band of $(\text{DF})_2$ is expected to be predominantly perpendicular, which is why Pine et al. observed the two $K = 1 \leftarrow 0$ subbands of ν_1 but not the corresponding $K = 0 \leftarrow 0$ subband.¹⁴ However, no rotational constants were previously reported for the $K = 1$ ν_1 level of $(\text{DF})_2$, and since both parallel

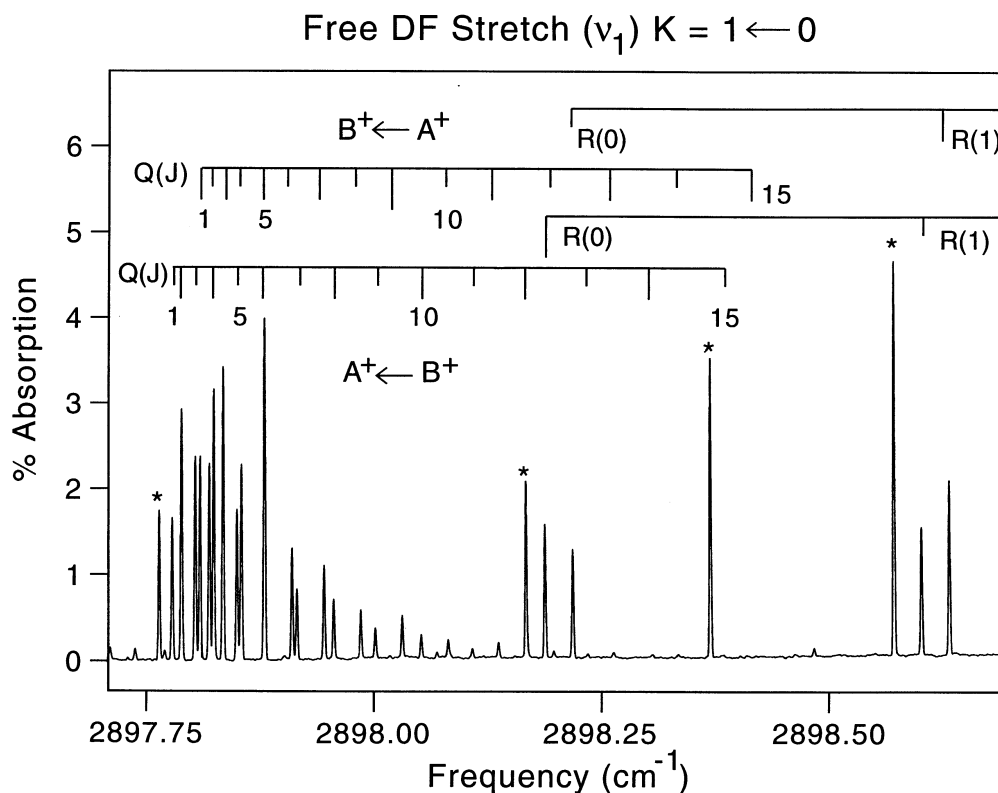


Figure 7.2 A section of the spectrum of the $K = 1 \leftarrow 0$ subband of the ν_1 band ($T_{\text{rot}} = 10 \pm 2$ K) of $(\text{DF})_2$. The A^+ and B^+ symmetry labels refer to $\Gamma_{\text{vib-tun}}$, the vibration-tunneling symmetry. Note the 7:5 spin statistical alternation in both bands and the narrow rovibrational linewidths. The transitions marked with an asterisk are due to ArDF clusters simultaneously formed in the expansion. Several small unassigned transitions scattered through out the spectrum are due to ν_1 “free” DF stretch excitation of DF-HF, which is present as “contaminant” due to incomplete deuteration of the mixing volumes.

and perpendicular bands were not observed the relative intensities could not be ascertained. Therefore, in the interest of completeness we have performed scans around the origins¹⁴ reported by Pine et al., which readily reveal intense absorptions ($S/N > 1000:1$) in the slit jet due to the perpendicular component ($K = 1 \leftarrow 0$) of ν_1 . Shown in Figure 7.2 is a sample spectral region containing the two Q branches and low J transitions of the two R branches for the different tunneling states. ArDF “contaminant” transitions (P(1) through R(2)) are marked with an asterisk, and the unassigned small features are due to DF-HF mixed dimer transitions.⁵¹ All of the $K = 1 \leftarrow 0$, ν_1 (DF)₂ transitions from R(9) to P(13) are reported in Table 7.1. The rotational progressions for each tunneling state are fit to Eq. (7.1) for the $\Gamma_{\text{vib-tun}} = B^+ \leftarrow A^+$ and $\Gamma_{\text{vib-tun}} = A^+ \leftarrow B^+$ bands, respectively, and the results summarized in Table 7.2. The residual standard deviation for fits to these high signal-to-noise bands is smaller than experimental uncertainty (0.0001 cm^{-1}), indicating the absence of any rotational perturbations. The tunneling splitting obtained for the $K=1$, ν_1 state is $0.02193(6) \text{ cm}^{-1}$, which is in good agreement with the $0.02220(60) \text{ cm}^{-1}$ value obtained from the reported origins of Pine.¹⁴ The improved agreement between the cooled cell and slit jet measured tunneling splittings for the perpendicular vs. parallel band is almost certainly due to the presence of a strong Q branch, which allows a more precise determination of origins even under the higher temperature cell conditions. The integrated intensity of this band is approximately 10-fold larger than the parallel band; this is in the same direction but even greater than the 5-fold ratio experimentally

observed¹⁹ in (HF)₂ and the factor of four predicted for a “free” H/DF stretch dipole transition moment evaluated at the equilibrium angular geometry.

7.3.4 ν_2 (“bound” DF stretch): $K = 0 \leftarrow 0$

Whereas the ν_1 mode is predominantly perpendicular (by roughly 5:1 in (HF)₂ and 10:1 in (DF)₂), the ν_2 (“bound” DF stretch) is expected to be a predominantly parallel band. Specifically, for a dipole moment aligned along the bound monomer in its equilibrium geometry,³¹ the perpendicular:parallel intensity ratio is predicted to be $\approx 1:40$. Indeed, for both HF and DF dimers no perpendicular bands of ν_2 have been observed,¹⁴ despite S/N in excess of 1000:1 on the corresponding parallel bands. To obtain *relative* intensities for the various ν_1 and ν_2 spectra, we have therefore performed scans around the (DF)₂ ν_2 origin, revealing the $K = 0 \leftarrow 0$ subband as by far the strongest of the intramolecular vibrational transitions. Figure 7.3 shows a sample P/R branch region of the spectrum. The transition frequencies are reported in Table 7.3. The rotational progressions for each tunneling level are fit to Eq. (7.1) for the $\Gamma_{\text{vib-tun}} = B^+ \leftarrow A^+$ and $\Gamma_{\text{vib-tun}} = A^+ \leftarrow B^+$ bands respectively; the results are summarized in Table 7.4. The residual standard deviations for both fits are $\leq 0.0001 \text{ cm}^{-1}$, i.e., no signs of perturbations are observed. The tunneling splitting from the current slit jet studies is measured to be $0.01741(7) \text{ cm}^{-1}$, which is slightly higher than the value of $0.01640(80) \text{ cm}^{-1}$ determined from the reported vibrational origins of Pine et al.¹⁴ This discrepancy is likely to be due to the absence of Q branches in a $K = 0 \leftarrow 0$

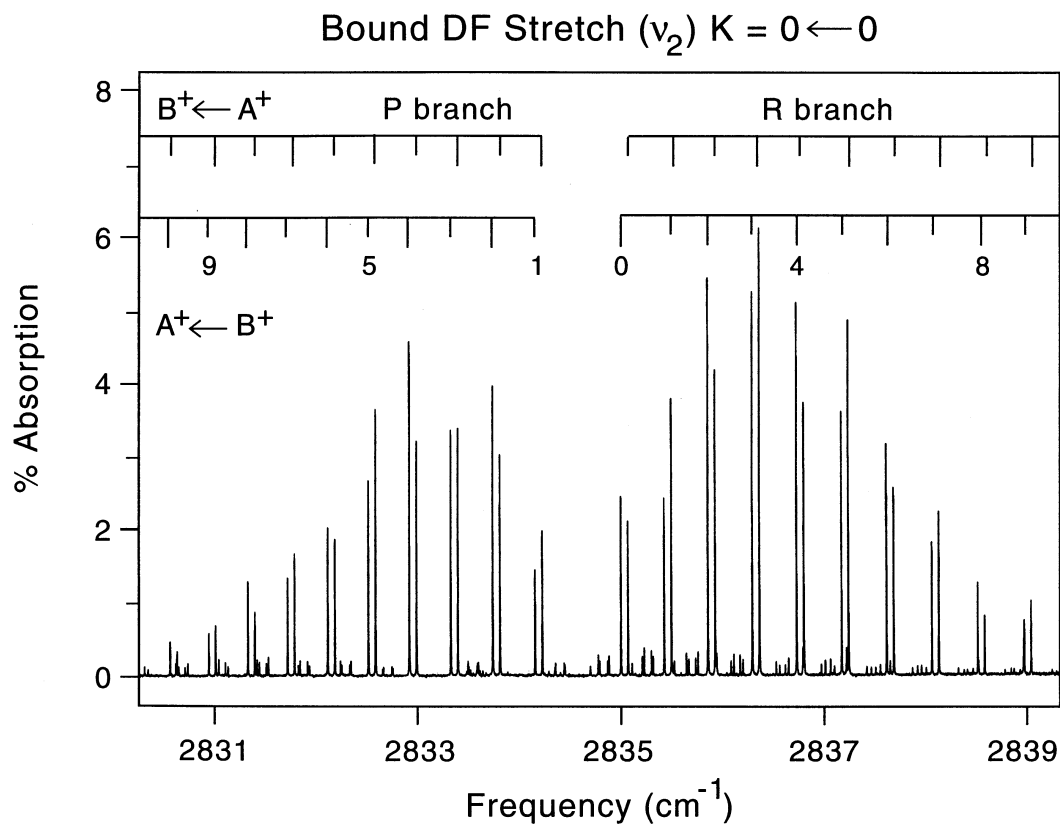


Figure 7.3 The $K = 0 \leftarrow 0$ subband of the ν_2 mode ($T_{\text{rot}} = 10 \pm 2$ K) of $(\text{DF})_2$. The A^+ and B^+ symmetry labels refer to $\Gamma_{\text{vib-tun}}$, the vibration-tunneling symmetry. The weaker transitions are due to both ν_2 DF stretch excitation in HF-DF and $K = 1 \leftarrow 1$ $(\text{DF})_2$ hot band transitions.

Table 7.3 The observed and fitted transition frequencies for ν_2 “bound DF stretch”. The numbers in parentheses represent the deviations (obs – calc) from the least-squares fit of each VRT band in units of the last reported digit. The absolute frequencies are determined by reference to P(3) of DF monomer at $2839.78537 \text{ cm}^{-1}$,^a with an accuracy of 0.0002 cm^{-1} .

$\Gamma_{\text{vib-tun}} =$	$\nu_2 \quad K = 0 \leftarrow 0$	
	$B^+ \leftarrow A^+$	$A^+ \leftarrow B^+$
R(15)	2841.78284(-10)	2841.71839(-8)
R(14)	2841.30847(-67) ^b	2841.24447(-4)
R(13)	2840.83897(7)	2840.77391(5)
R(12)	2840.37215(2)	2840.30658(3)
R(11)	2839.90894(16)	d
R(10)	2839.44894(10)	2839.38201(-3)
R(9)	2838.99233(3)	2838.93376(-13)
R(8)	2838.53910(-7)	2838.47110(-9)
R(7)	2838.08945(-1)	2838.02092(-6)
R(6)	2837.64314(-7)	2837.57426(-3)
R(5)	2837.20039(-5)	2837.13119(3)
R(4)	2836.76116(-5)	2836.69162(-1)
R(3)	2836.32556(2)	2836.25573(0)
R(2)	2835.89351(2)	2835.82347(-5)
R(1)	2835.46514(3)	2835.39504(2)
R(0)	2835.04056(14)	2834.97039(10)
P(1)	2834.20246(9)	2834.13224(-4)
P(2)	2833.78912(2)	2833.71911(2)
P(3)	2833.37927(0)	2833.30988(3)
P(4)	2832.97422(-6)	2832.90460(0)
P(5)	2832.57281(-2)	2832.50347(6)
P(6)	2832.17545(3)	2832.10630(0)
P(7)	2831.78198(-13)	2831.71331(-3)
P(8)	2831.39293(-2)	2831.32458(1)
P(9)	c	2830.94002(-4)
P(10)	2830.62723(-12)	2830.55984(-1)
P(11)	c	2830.18399(-3)
P(12)	c	2829.81272(11)
P(13)	2829.51109(-99) ^b	c
P(14)	2829.14765(-195) ^b	2829.08352(22)

Table 7.3 continued

$\Gamma_{\text{vib-tun}}$	$v_2 K = 1 \leftarrow 1$			
	$B^+ \leftarrow A^+$		$A^+ \leftarrow B^+$	
	Lower \leftarrow Lower	Upper \leftarrow Upper	Lower \leftarrow Lower	Upper \leftarrow Upper
R(15)				
R(14)				
R(13)				
R(12)	2839.28328(1)	2839.34753(57) ^b	2839.19653(-5)	2839.26279(9)
R(11)	2838.82431(-14)	2838.88435(121) ^t	2838.73632(82) ^b	2838.79762(-12)
R(10)	2838.36890(17)	2838.42243(5)	2838.28094(7)	2838.33604(2)
R(9)	2837.91619(5)	2837.96453(-22)	2837.82794(13)	2837.87745(-12)
R(8)	2837.46691(20)	2837.51036(8)	2837.37790(-5)	2837.42244(5)
R(7)	2837.02031(-15)	2837.05911(9)	2836.93123(-10)	2836.97064(11)
R(6)	2836.57755(11)	2836.61084(-16)	2836.48787(-10)	2836.52195(-6)
R(5)	2836.13779(12)	2836.16609(-18)	2836.04798(6)	2836.07684(0)
R(4)	2835.70114(-5)	2835.72484(-3)	2835.61109(-10)	2835.63516(7)
R(3)	2835.26806(3)	2835.28679(-7)	2835.17792(9)	2835.19690(12)
R(2)	2834.83829(5)	2834.85225(-1)	2834.74803(15)	2834.76188(-9)
R(1)	2834.41184(0)	2834.42087(-25)	2834.32131(-6)	2834.33055(-12)
R(0)				
P(1)				
P(2)	2832.74130(18)	2832.73223(10)	2832.65066(4)	2832.64166(-3)
P(3)	2832.33247(11)	2832.31904(4)	2832.24174(-23)	2832.22876(4)
P(4)	2831.92703(-24)	2831.90975(15)	2831.83722(19)	2831.81953(-4)
P(5)	2831.52593(5)	2831.50386(-11)	2831.43580(-3)	2831.41422(-5)
P(6)	2831.12817(-7)	2831.10222(4)	2831.03852(9)	c
P(7)	2830.73436(-6)	2830.70444(18)	2830.64489(0)	2830.61575(28)
P(8)	2830.34437(-8)	2830.31037(11)	c	2830.22196(-13)
P(9)	2829.95806(-34)	2829.92041(17)	c	2829.83272(-9)
P(10)	2829.57666(35)	2829.53426(3)	2829.48764(-26)	c
P(11)	2829.19802(-22)	2829.15210(-18)	2829.10033(1)	2829.06681(3)
P(12)	2828.82353(-72) ^b	2828.77458(12)	2828.73726(34)	c
P(13)		2828.40232(151) ^t	2828.36758(-17)	2828.31731(-69) ^b
P(14)				

a. Reference 45.

b. not included in the fit.

c. overlap between $K=0\leftarrow 0$ and $K=1\leftarrow 1$ transition in v_2

d. overlap with HF-DF transition

Table 7.4 Molecular constants (cm^{-1}) determined from fits of the transition frequencies to Eq. (7.1) for ν_2 “bound DF stretch” bands. The uncertainties in parentheses represent 2σ , from the least squares fit, in the units of the last reported digit.

$\Gamma_{\text{vib-tun}} =$	$\nu_2 \quad K = 0 \leftarrow 0$		$\nu_2 \quad K = 1 \leftarrow 1$	
	$B^+ \leftarrow A^+$	$A^+ \leftarrow B^+$	$B^+ \leftarrow A^+$	$A^+ \leftarrow B^+$
\mathbf{n}_0	2834.61949(6)	2834.54936(4)	2833.56944(10)	2833.47886(12)
\bar{B}'_K	0.2104665(14)	0.2104693(12)	0.210888(4)	0.210902(8)
$b'_K/10^{-3}$	----	----	4.604(8)	4.61(4)
$D'_K/10^{-6}$	1.941(6)	1.880(2)	1.82(2)	1.85(4)
$d'_K/10^{-6}$	----	----	0.10(4)	0.15(6)
σ_{rms}	0.00008	0.00007	0.0002	0.0001

parallel band, which makes the present determination of vibrational origins from P/R branch fits to the low J states populated under supersonic jet conditions more accurate. The integrated intensity of this band is a factor of 5- and 50-fold greater than the integrated intensity of the perpendicular and parallel ν_1 bands, respectively.

7.3.5 ν_2 (“bound” DF stretch): $K = 1 \rightarrow 1$

Close inspection of the $K = 0 \leftarrow 0$ subband of ν_2 shown in Figure 7.3 also reveals a large number of weaker transitions. Although some of these transitions in the R branch are due to HF-DF mixed dimer peaks,⁵¹ most can be ascribed to the parallel $K = 1 \leftarrow 1$ ν_2 band of $(\text{DF})_2$. Shown in Figure 7.4 is a close up of the

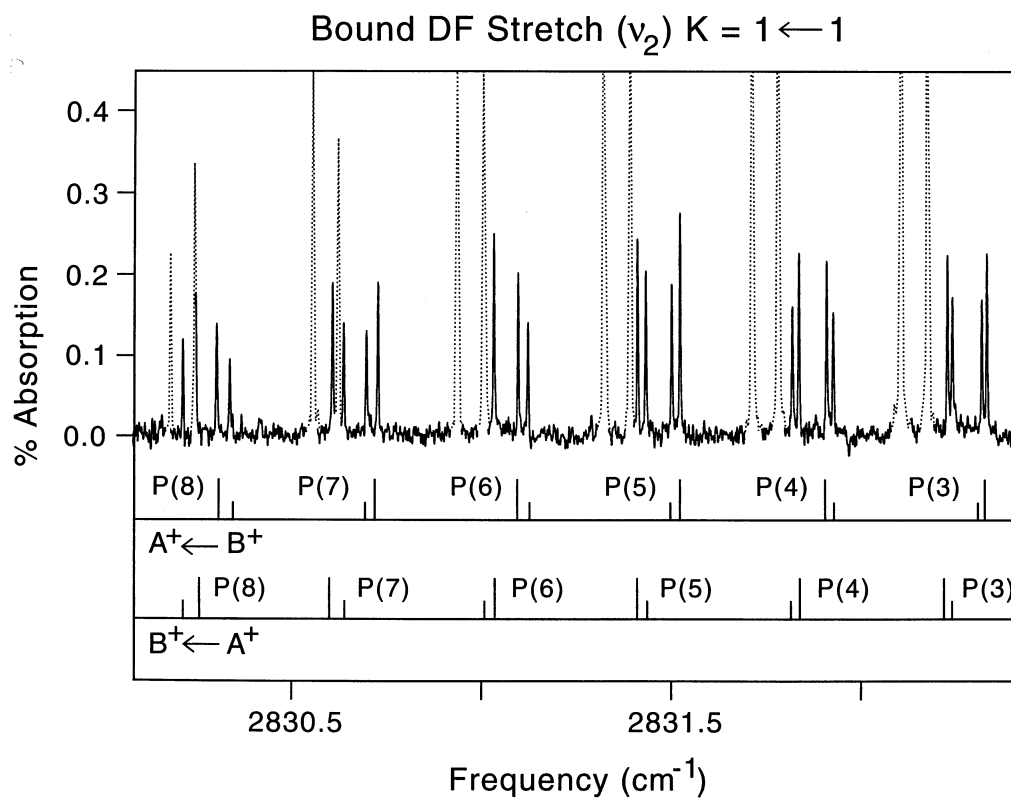


Figure 7.4 Spectral region displaying the P branch of the $K = 1 \leftarrow 1$ subband of ν_2 . Note the fourfold splitting of each state due to i) A^+/B^+ tunneling splitting and ii) asymmetry splitting in both the $K = 1$ ground and excited state. The spectral features drawn with a dotted line correspond to the $K = 0 \leftarrow 0$ ν_2 band shown in Figure 7.3.

above spectrum which readily demonstrates a repeated rotational progression of four peaks, arising from a combination of both i) $K = 1$ asymmetry and ii) A^+/B^+ tunneling splittings. The already assigned and much stronger $K = 0 \leftarrow 0$ transitions have been marked with dotted lines for visual clarity. Combination differences verify that this progression of weaker transitions originate from the $K = 1$ level of the $(DF)_2$ ground state. Excitation of the ν_2 “bound” DF stretch corresponds to a change in the dipole moment nearly aligned with the A molecular axis; in asymmetric top language this corresponds to a predominantly A -type band, where the appropriate selection rules are $\Delta K_a = 0, \pm 2, \dots$ and $\Delta K_c = \pm 1, \pm 3, \dots$. For the near symmetric top energy level expression employed in this study, the $K = 1$ asymmetry selection rules are simply lower level-to-lower, and upper-to-upper. The frequencies for all of the observed transitions are reported in Table 7.3. The rotational progressions are fit to Eq. (7.1) for the $\Gamma_{\text{vib-tun}} = B^+ \leftarrow A^+$ and $\Gamma_{\text{vib-tun}} = A^+ \leftarrow B^+$ bands respectively. The residual standard deviation for both fits is $\leq 0.0002 \text{ cm}^{-1}$. The tunneling splitting for the $K = 1, \nu_2$ state is $0.0218(2) \text{ cm}^{-1}$, which is 25% larger than the corresponding $K = 0 \nu_2$ state. The integrated intensity of this band is approximately a factor of 10 lower than the integrated intensity of the $\nu_2 K = 0 \leftarrow 0$ band; this is simply due to the reduced Boltzmann population of a 16 cm^{-1} “excited” $K = 1$ state in the 8-10 K slit jet expansion.

The above analysis of the $K = 1 \leftarrow 1$ subband of ν_2 provides a direct measure of rotational constants, tunneling splittings, and (as discussed in Section 7.4) vibrational predissociation for the $\nu_2, K = 1$ excited state. In conjunction with the vibrational ground state K spacing, as determined from $\nu_1, K = 0 \leftarrow 0$ and $K =$

$0 \leftarrow 1^4$ subbands, the vibrational origin for the ν_2 , $K=1 \leftarrow 1$ subband provides the K spacing in the ν_2 excited state. This information could have alternatively been obtained from scans over the perpendicular, $K = 1 \leftarrow 0$, ν_2 subband; however, survey scans over the ν_2 perpendicular absorption region reveal no transitions. With accurate determination of the ν_2 K spacing from the $K = 1 \leftarrow 1$ data, careful scans have been repeated in the exact region where the ν_2 , $K = 1 \leftarrow 0$ bands must occur; again no transitions are observed, despite a complete absence of spectral congestion in the jet and a S/N in excess of 1000:1 on the corresponding ν_2 , $K = 0 \leftarrow 0$ parallel bands. Since the $K = 1 \leftarrow 1$ data already measures the spectral linewidths, this eliminates from consideration that the ν_2 $K = 1$ upper state is excessively broadened; the parallel:perpendicular intensity ratio for ν_2 must therefore be at least $\geq 1000:1$. It is worth noting that a similar absence of perpendicular intensity in the ν_2 band was also observed⁵¹ in slit jet studies of $(\text{HF})_2$. In both isotopomers, the observed ratios are significantly greater than the 40:1 ratio predicted from a “bound” H/DF stretch dipole transition moment and an equilibrium geometry.

7.4 Discussion

7.4.1 Intramolecular excitation and vibrationally averaged structures

Due to the large amplitude intermolecular motion on the hydrogen bond potential surface, the more familiar notion of a classical “structure” is not well

defined, and needs to be replaced by expectation values of quantities that have been vibrationally averaged over both high frequency (*intramolecular*) and low frequency (*intermolecular*) degrees of freedom. Furthermore, due to the coupling on the potential energy surface between high and low frequency degrees of freedom, excitation of *intramolecular* modes in the HF or DF subunit can lead to appreciable changes in these vibrational averages. One quantitative measure of vibrationally averaged “structure” is provided by the spectroscopically derived rotational constants. Though somewhat indirect, these constants provide expectation values of rotational operators over even highly delocalized wavefunctions, and thus can offer insight into the general trends. For example, the \bar{B} rotational constant for a 4-atom system such as HF or DF dimer is dominated by the vibrationally averaged distance (more specifically, $\left\langle \frac{1}{R^2} \right\rangle$) between the two monomer centers of mass. Conversely, the effective *A* rotational constant (which we define as the energy difference between $K = 1$ and $K = 0$ vibrational origins) is dominated by H/D atom moments of inertia projected along the F-F axis, and thus provides a measure of the “bent” vs. “linear” nature of the hydrogen bond.

Shown in Figure 7.5 is a summary of the \bar{B} rotational constants for both the $K = 0$ and $K = 1$ intramolecular states, averaged over the two A^+/B^+ tunneling levels. The rotational constants are plotted as a function of the vibrational redshift, since this redshift is a measure of the differential strengthening of the hydrogen bond with ν_1 and ν_2 excitation. The trend in the \bar{B} constants for $(DF)_2$

Dependence of Rotational Constants on Intramolecular Vibration

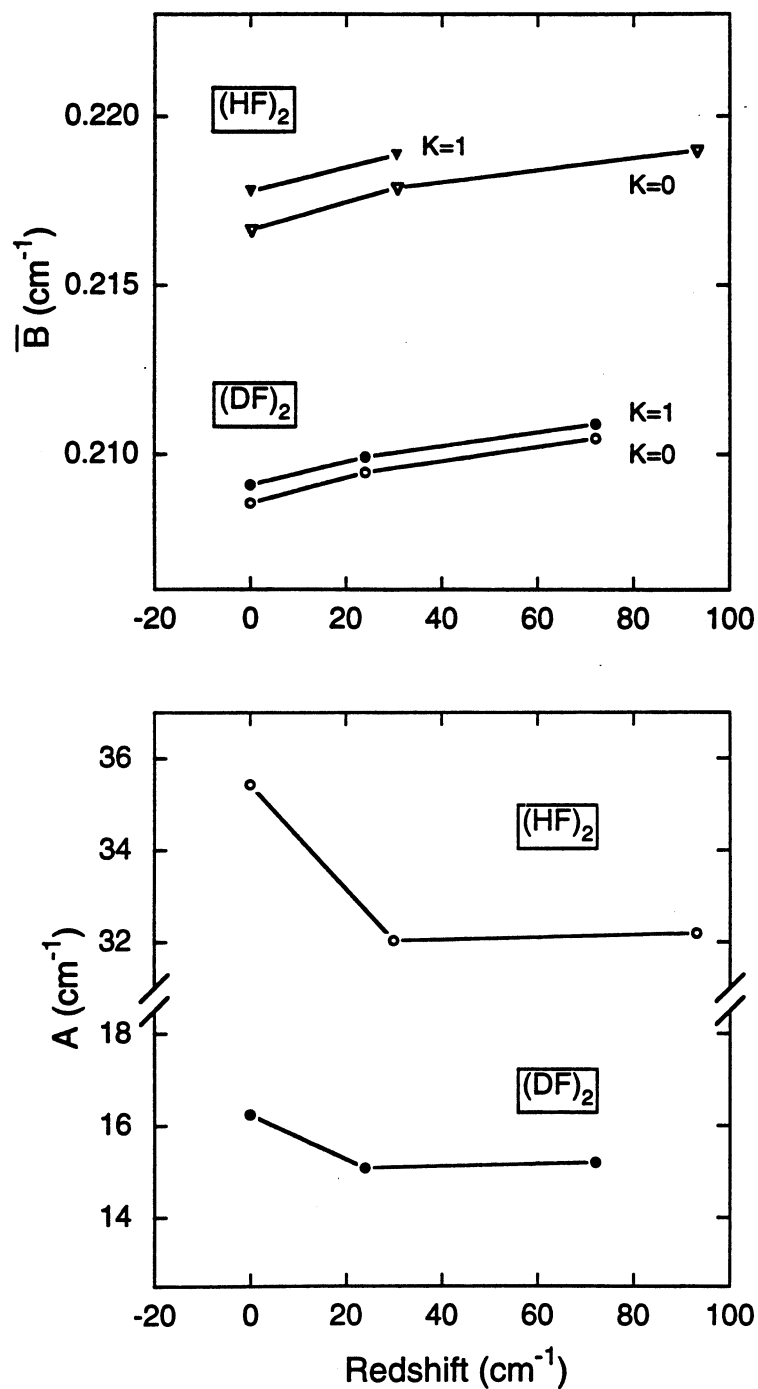


Figure 7.5 Plots of the experimentally observed rotational constants for $(\text{HF})_2$ and $(\text{DF})_2$ as a function of intramolecular vibrational redshift, where zero redshift corresponds to the ground state. The systematic increase in \bar{B} and decrease in A correspond to a shrinking and bending of the hydrogen bond, respectively, with intramolecular vibrational excitation.

is consistent with previously measured^{4,14} (HF)₂ trends, corresponding roughly to a 0.5% radial contraction as the hydrogen bond strength increases for both (HF)₂ and (DF)₂ species. This is qualitatively different than what is observed in the analogous hydrogen chloride dimer systems,^{8,52} where the \bar{B} for (HCl)₂ and \bar{B} for (DCl)₂ increase and decrease, respectively, upon intramolecular excitation.

However, it is worth noting that the magnitude of both the shifts in \bar{B} and vibrational origins upon ν_1 or ν_2 excitation in (HCl)₂ or (DCl)₂ are significantly smaller (\approx 40-fold) than the corresponding changes in (HF)₂ or (DF)₂, and thus may be more sensitive to additional vibrational averaging effects due to short range repulsive interactions.

Since the necessary $K = 1 \leftarrow 0$, $K = 0 \leftarrow 0$, $K = 1 \leftarrow 1$, and $K = 0 \leftarrow 1$ vibrational origins have been recorded for both HF^{4,14} and DF dimer, information on A may be determined for each vibrational state. Shown in Figure 7.5 is a plot of A vs. vibrational redshift. Note that upon intramolecular excitation A decreases \approx 10% for both isotopes, which corresponds roughly to a 5% increase in the moment of inertia about the A intermolecular axis. Given the 10-fold smaller changes in \bar{B} , this reflects a greater angular sampling of the “free” HF or DF monomer tilted further away from the F-F intermolecular axis. To account for the observed changes, the vibrationally averaged position of the “free” monomer must bend by roughly 10 degrees. It is interesting to note that this effect does not scale linearly with the strength of the hydrogen bond (i.e. vibrational redshift), as was observed for the \bar{B} rotational constants. Furthermore, this propensity for a shift

in equilibrium intermolecular bend angle with intramolecular stretching excitation is *not* accounted for in state-of-the-art 6-D potential energy surfaces,³¹ which predict only negligible (less than a few degrees) shifts in the equilibrium hydrogen bond bend angle for as much as 0.1 Å stretching of the monomer subunits.

7.4.2 Isotopic and *K* dependence of tunneling splittings

It has long been appreciated that the (HF)₂ and (DF)₂ potential energy surface has two isoenergetic minima that are most directly connected through a “geared” bending motion of the two monomers. The barrier separating these two minima is estimated¹⁴ to be only 300-350 cm⁻¹, which permits significant tunneling probabilities for motion of the two hydrogen or deuterium atoms. This tunneling phenomenon manifests itself spectroscopically as a splitting of each rovibrational eigenstate, as experimentally first observed for both isotopes by Dyke et. al.⁹ As noted in the near IR difference frequency laser studies of Pine et al.,¹⁴ vibrational excitation of one of the monomers significantly diminishes the tunneling rates; a factor of 3 decrease in tunneling splitting was observed for both isotopes upon intramolecular excitation. The trends and magnitude of these tunneling splittings as a function of vibrational excitation provide a stringent test of trial potential energy surfaces,³⁸ and have been the subject of much theoretical investigation.^{14,31-35,38,40,47,53-59} For example, the novel “quenching” of tunneling rates upon intramolecular excitation has stimulated interpretations based on resonant *intermolecular* V-V transfer at the tunneling transition state,⁵⁹ or equivalently,

Table 7.5 Tunneling splittings (cm^{-1}) for HF and DF dimers. The uncertainties in parentheses represent 2σ in the units of the last reported digit.

		$K = 0$	$K = 1$
	ν_0	0.0527207(14) ^a	0.0688066(8) ^a
(DF) ₂	ν_1	0.01668(14)	0.02193(6)
		0.01630(70) ^b	0.02220(60) ^b
	ν_2	0.01741(7)	0.0218(2)
		0.01640(80) ^b	
	ν_0	0.6586902(10) ^a	1.0644376(8) ^a
(HF) ₂	ν_1	0.2150(9) ^b	0.3498(3) ^b
	ν_2	0.2336(7) ^b	0.3414(19) ^b

a Reference 12

b Obtained from vibrational origins reported by Pine et al. (ref. 14).

non-adiabatic surface “crossings” between two Born-Oppenheimer surfaces formed from vibrationally excited subunits. More recently, a coupled local oscillator model has also been used successfully to predict both vibrational and isotopic trends in tunneling splittings.⁶⁰

With the current set of measurements, accurate tunneling splittings now exist for both $K = 0, 1$ levels of (HF)₂ and (DF)₂ in the ground, ν_1 and ν_2 excited states. As can be seen from Table 7.5, the tunneling splittings increase consistently with K excitation for both isotopes and both intramolecular vibrations, $\approx 60\%$ and $\approx 30\%$ for (HF)₂ and (DF)₂, respectively. This strong K dependence has been noted previously in (HF)₂ and interpreted on the basis of

centrifugal “bending” of the dimer subunits towards the tunneling transition state.¹⁴ Explicitly, the instantaneous moment of inertia around the A axis is strongly dependent on the intermolecular geared bend coordinate, increasing dramatically towards the tunneling transition state. Thus, tunneling for the $K = 0$ and 1 levels can be thought as taking place on different adiabatic potentials with barrier heights that differ by approximately ΔA , where this reflects the difference in “instantaneous” A constants evaluated at the minimum and transition state region.

This model can be extended to predict the H vs. D isotope dependence of these centrifugal enhancements. Based on an assumed potential such as the SQSBDE surface³¹ of Quack and Suhm, the A constant can be calculated at both the equilibrium and transition state geometries for each isotopomer; the difference in A values would then correspond to the predicted decrease in the 1-D barrier height. The calculated decrease in A is 11.7 cm^{-1} for $(\text{HF})_2$ and only 6.4 cm^{-1} for $(\text{DF})_2$, i.e., this model correctly predicts a *larger* K effect in the H vs. D isotopomer.

We can estimate the magnitude of this effect from a simple semiclassical WKB analysis of motion over the barrier. For a parabolic barrier it is straightforward to derive the WKB tunneling rates⁶¹

$$\Delta n_{\text{tun}} = \left(\frac{n_0}{p} \right) \exp \left[\frac{-2p^2}{h} \sqrt{\frac{2m}{k}} E^\ddagger \right] \quad (7.3)$$

where \mathbf{n}_0 is the geared bend vibrational frequency, μ is the effective tunneling mass, \mathbf{k} is the force constant for the parabolic barrier maximum, and E^\ddagger is the height of the barrier from the zero point level. Since neither \mathbf{k} nor \mathbf{n}_0 is known, Eq. (7.3) is not useful for obtaining E^\ddagger . However, if we make the plausible assumptions that i) the geared bend frequency \mathbf{n}_0 does not change significantly upon K excitation, and ii) \mathbf{k} is the same for (HF)₂ and (DF)₂ in both $K = 0$ and $K = 1$, then K dependent logarithmic ratios of Eq. (7.3) can provide some comparison with the experimental numbers. Specifically, the ratio between

$$\Delta \mathbf{n}_{1,0} \equiv \ln \left(\frac{\Delta \mathbf{n}_{\text{tun}}^{K=1}}{\Delta \mathbf{n}_{\text{tun}}^{K=0}} \right) \text{ for (HF)}_2 \text{ and (DF)}_2 \text{ can be used to eliminate the dependence}$$

on both \mathbf{n}_0 and \mathbf{k} , resulting in the prediction

$$\frac{\Delta \mathbf{n}_{1,0}^{HF}}{\Delta \mathbf{n}_{1,0}^{DF}} = \sqrt{\frac{\mathbf{m}_{HF}}{\mathbf{m}_{DF}}} \left(\frac{\Delta E_{\text{barrier}}^{HF}}{\Delta E_{\text{barrier}}^{DF}} \right) \quad (7.4)$$

where μ_{HF} and μ_{DF} are the effective masses for the tunneling motions in both isotopes. Though not quantitatively predictive, the form of Eq. (7.4) offers some interesting insights because it isolates the K and isotopic dependence of tunneling rates into two competing factors, i.e. effective tunneling mass and barrier height.

For strictly “geared” tunneling motion, $\frac{\mathbf{m}_{HF}}{\mathbf{m}_{DF}}$ would equal the ratio of HF and DF

monomer B constants, while $\Delta E_{\text{barrier}}^{HF}$ and $\Delta E_{\text{barrier}}^{DF}$ are the decreases in the 1-D

barrier heights predicted upon $K = 1 \leftarrow 0$ excitation, namely, $\Delta A = 11.7$ and 6.4 cm^{-1} , respectively. From these values, Eq. (7.4) predicts a ratio of 1.33, which is in

reasonable qualitative agreement with experimental results of 1.78, 1.77 and 1.72 for the ground state, ν_1 and ν_2 , respectively.

The WKB analysis presented above only addresses the greater increase in tunneling splitting upon K excitation for HF vs. DF dimer. An equally intriguing trend is the factor of 3 *decrease* in $\Delta\nu_{\text{tun}}$ upon intramolecular excitation observed in *both* isotopes. This isotopic invariance was first reported by Pine et al.¹⁴ and phenomenologically interpreted as a preferential increase in an effective barrier to inversion for (HF)₂ vs. (DF)₂. This trend was successfully predicted, for both isotopes, by the quantum exchange model of Fraser,⁵⁹ which is based on the physically reasonable assumption of resonant *intermolecular* V-V transfer between the subunits at the tunneling transition state. Recently, Chang and Klemperer⁶⁰ have proposed a coupled local oscillator picture to model both tunneling and vibrational predissociation in these hydrogen bonded dimers. Specifically, they represent the Hamiltonian in a direct product basis of “left” and “right” orientations, differing by which subunit participates in the hydrogen bonding, and localized vibrations on each monomer. Coupling between “left” and “right” orientation elements, in both the ground and vibrationally excited states, produces the tunneling splittings, and is used to fit relevant off diagonal matrix elements. Interestingly, isotopic scaling of this simple model correctly predicts both the factor of 3 decrease upon vibrational excitation and the invariance of this decrease in (HF)₂ and (DF)₂. However, this more phenomenological treatment does not specifically rely on or identify any physical mechanism for V-V transfer, unlike the quantum exchange model of Fraser.⁵⁹

7.4.3 Vibrational predissociation

The dissociation energy for HF dimer has been measured by photofragment translational spectroscopy to be $1062(1) \text{ cm}^{-1}$.¹⁷ Though not yet experimentally measured for DF dimer, D_0 has been predicted³¹ from full 6-D quantum calculations on the SQSBDE potential surface to be 1169 cm^{-1} . Both values are significantly below the intramolecular HF/DF stretch frequencies, and thus “free” and “bound” ν_1 and ν_2 intramolecular excited states in HF and DF dimer are sufficiently energetic to rupture the hydrogen bond. One therefore anticipates predissociation broadening to be evident in the spectrum, with a magnitude that is sensitive to the rate of unimolecular energy flow from high frequency (*intramolecular*) to low frequency (*intermolecular*) degrees of freedom. Experimental measurements of these rates provide a stringent test of trial potential energy surfaces as well as for theoretical models of unimolecular energy flow dynamics in hydrogen bonded systems.

For HF dimer, vibrational predissociation has been observed and extensively studied, both experimentally^{4,14,17-22,37,62,63} and theoretically.^{36,39-41} Fraser and Pine¹⁹ have measured predissociation broadening in both intramolecular modes and find that the ν_2 “bound” HF stretch predissociates approximately 30/50 times faster for antisymmetric/symmetric tunneling states than the ν_1 “free” HF stretch, even though ν_1 excitation occurs at a higher frequency and thus provides more excess energy to the dissociating complex. This mode specificity has been interpreted as arising from stronger coupling of the “bound” ν_2 stretch

(DF)₂ Vibrational Predissociation

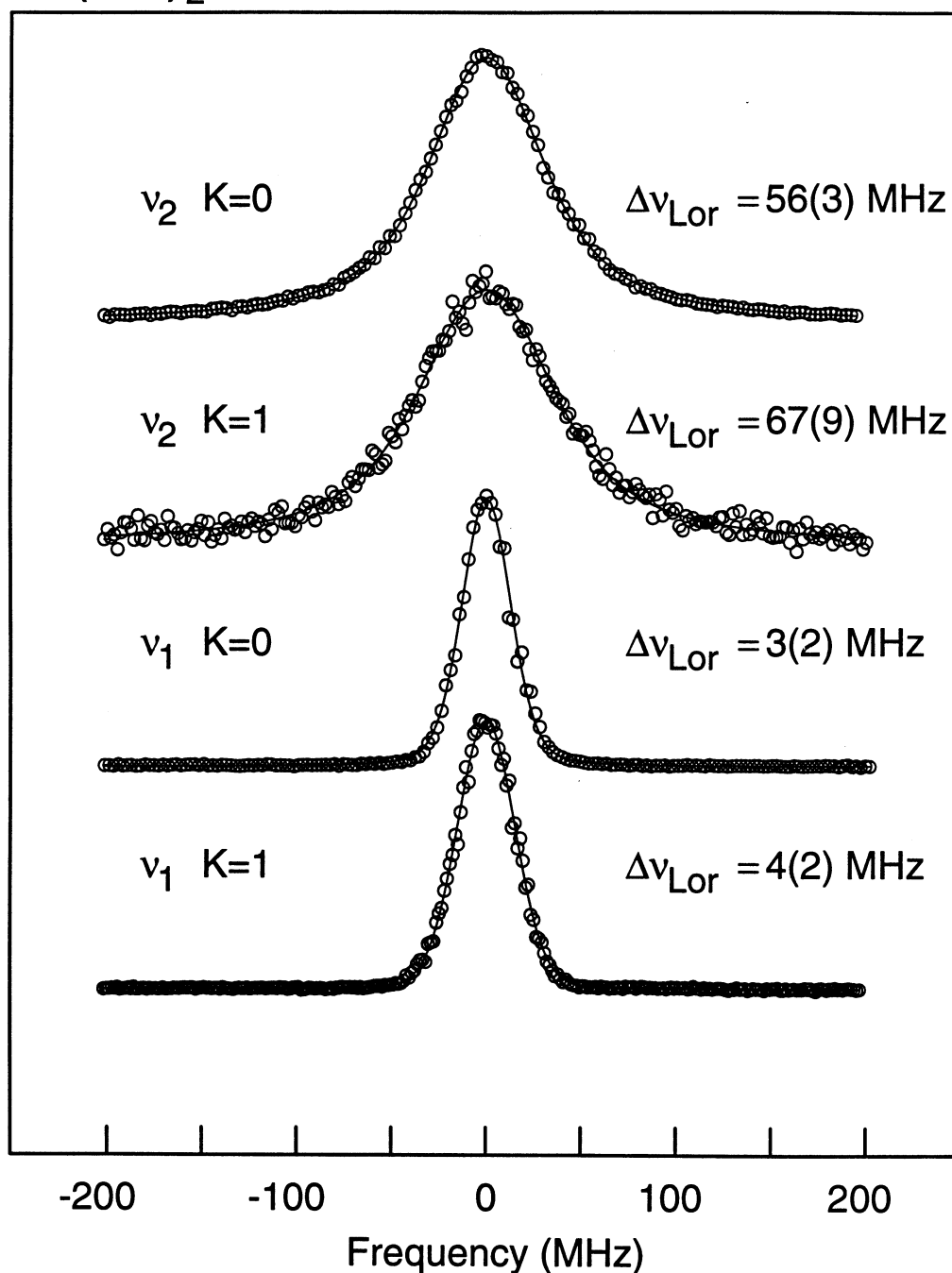


Figure 7.6 Sample lineshape data for $K = 0$ and $K = 1$ states of both ν_1 and ν_2 intramolecular modes (for $\Gamma_{\text{tun}} = B^+$ upper levels). The solid line through the data represents the corresponding least squares fits to a Voigt profile. The Lorentzian component for each fit is indicated in MHz. Note the 20-fold mode specific *increase* in predissociation rates between “free” ν_1 and “bound” ν_2 vibrational excitation. This is quite close to the ratio observed for (HF)₂ and in good agreement with the absence of an H/D isotope effect predicted by Chang and Klemperer.⁶⁰

with the dissociation coordinate. This interpretation of predissociation rates being controlled by dynamical rather than statistical processes was further supported by product state resolved experiments of Miller and coworkers,^{17,18} which suggested a propensity for strongly correlated (high j -low j) product states, despite the presence of nearly resonant channels to yield HF + HF with more equivalent levels of rotational excitation. Both the ν_1/ν_2 mode specificity and the high j -low j product correlation suggest an impulsive predissociation event, i.e., the intramolecular excited states couple directly with the dissociation continuum, rather than the energy first flowing into highly excited overtones and combination levels of the hydrogen bond intermolecular vibrational manifold.

A further test of such dynamical interpretations of the predissociation event can be obtained from the present isotopic substitution studies. In the early work of Pine et al.,¹⁴ high resolution scans over ν_1 and ν_2 transitions of (DF)₂ were obtained, but under these equilibrium cooled cell conditions, the experimental linewidths were on the order of ≈ 100 MHz, dominated by a combination of Doppler and residual pressure broadening. Nevertheless, this permitted them to set a lower limit on the (DF)₂ ν_1 and ν_2 predissociation lifetimes of 10 nsec, which is already considerably longer than the measured ν_2 value (530 ± 50 psec) for (HF)₂. In the present study, pressure broadening due to collisions in the supersonic expansion is negligible, and the Doppler widths are reduced by 10-fold from room temperature values due to collimation in the slit jet geometry. Furthermore, from lineshape analysis of non-predissociating species in the supersonic jet, we can directly measure non-Doppler contributions to the

instrumental lineshape, which allows extraction of predissociation broadening rates at the level of a few MHz. As a result, the present experiment is able to probe considerably longer vibrational predissociation lifetimes than previously possible from cooled cell studies.

The details of experimental linewidth measurements with the present apparatus have been presented elsewhere.⁶⁴ Briefly, the observed lineshapes can be well approximated as a Voigt convolution of a Gaussian and Lorentzian profile. The Gaussian component is due predominantly to residual Doppler contributions at the slit jet temperature. The Lorentzian component is due predominantly to vibrational predissociation with 1-2 MHz contribution from laser jitter and slit jet edge effects. Small stepsize (1.4 MHz) scans over several rotational transitions for each vibration are recorded. The lineshapes are least squares fit to a Voigt profile with both the Gaussian and Lorentzian widths independently floated. The Gaussian widths are then averaged ($\Delta\nu_{\text{Gau}} = 30(5)$ MHz), and the lineshapes refit with the Gaussian width fixed at this average to extract the Lorentzian component ($\Delta\nu_{\text{Lor}}$). Figure 7.6 shows sample lineshape data for each intramolecular vibration and $K = 0, 1$ state, along with the corresponding Voigt fits. The results of this analysis are summarized in Table 7.6. The uncertainties reported in the table correspond to the standard deviation of multiply repeated measurements, rather than the much smaller standard deviation of the mean.

Table 7.6 Lorentzian linewidths for (DF)₂ ν_1 and ν_2 bands in MHz. The uncertainties in parentheses represent 1σ , obtained from repeated measurements, in the units of the last reported digit.

		$K=0$		$K=1$	
		A ⁺	B ⁺	A ⁺	B ⁺
(DF) ₂	ν_1	3(2)	3(2)	4(2)	4(2)
	ν_2	57(2)	56(3)	68(7)	67(9)
(HF) ₂	ν_1	6.4(5) ^a	9.5(5) ^a	10.2(5) ^a	11.8(5) ^a
	ν_2	330(30) ^a	330(30) ^a		

a. Reference 19

First of all, the data indicate that vibrationally excited (DF)₂ does indeed predissociate, and with a K and ν_1/ν_2 mode dependence similar to what has been observed in (HF)₂. Linewidths range from 3(2) MHz for $K = 0$, ν_1 to 68(7) MHz for $K = 1$, ν_2 excitation, corresponding to predissociation lifetimes from 50(30) to 2.3(1) nsec, respectively. Several different J 's for each vibration have been sampled, with no appreciable J dependence detected. Likewise, both tunneling states are sampled and indicate identical predissociation linewidths within experimental uncertainty. It is worth noting that the $\Delta_{\nu_{\text{lor}}}$ values for the $K = 0$ ν_1 upper states are comparable to the 1-2 MHz instrumental contribution, and thus do not explicitly rule out the possibility of much longer predissociation lifetimes. However, the high S/N and large number of measurements (>50) strongly suggest that the mean value of 3 MHz reflects significant contributions from predissociation.

Secondly, there is a clear mode specificity in vibrational predissociation rates observed for DF dimer, varying by at least 20 fold between ν_1 and ν_2

excitation. This is quite similar to the 30-50 fold difference in rates observed in HF dimer,¹⁹ and lends further credence to an impulsive model of the predissociation event. Specifically, if a fortuitous energy resonance were responsible for the ν_1/ν_2 mode specificity in HF dimer, then energy shifts upon isotopic substitution would make it improbable to reproduce such a similar behavior in DF dimer. Additionally, this consistent trend for the two isotopomers further absolves local fluctuations in the densities of product state channels, which would tend to *decrease* rather than *increase* predissociation rates for ν_1 vs. ν_2 excitation. While the trend is reproduced in both isotopes the magnitude of the effect may be smaller for (DF)₂. Such a decreased ν_1/ν_2 mode specificity in DF vs. HF dimer was predicted by Pine¹⁶ based on simple reduced mass considerations; the normal mode fluorine displacements are roughly twice as large for DF, which could result in an increased kinetic coupling of the ν_1 stretch to the hydrogen bonding region and thus a reduced ν_1/ν_2 mode specificity. Interestingly, if one assumes that only the localized, “bound” H/DF stretch couples with the dissociation coordinate, this mode specificity is predicted nearly quantitatively for both isotopes by the coupled local oscillator model of Chang and Klemperer.⁶⁰ In essence, the model predicts the ν_1 upper state for both isotopomers to exhibit 96%:4% mixed “free” and “bound” state character, which would suggest ν_1/ν_2 predissociation rates in the same ratio. While these predictions of the coupled local oscillator model are consistent with the mode specificity observed experimentally, it is worth mentioning that the model appears to be inconsistent with observed intensities. Specifically, the ν_2 mode would be predicted to derive

$\approx 4\%$ of its oscillator strength from the predominantly perpendicular “free” H/DF stretch, which is inconsistent with the experimentally observed ≥ 1000 -fold decrease in intensity from the parallel band. Also interesting to note is the dependence of predissociation rate upon K , which is similar (although a bit smaller) than the K dependence previously observed in HF dimer. Pine and Fraser have discussed¹⁹ this K dependence in HF dimer and described how a simple geometric picture, based on a change in geometry upon K excitation, fails to predict the correct sign of the effect.

Thirdly, the vibrational predissociation linewidths in hydrogen fluoride dimer decrease significantly upon deuteration, which can be interpreted *qualitatively* within the framework of energy gap predissociation models presented by Ewing.⁶⁵ Specifically, the initial vibrational energy deposited in the complex scales with the *square root* of HF/DF reduced mass, whereas the rotational energy necessary for dissociation into a given j scales *linearly* with this reduced mass. In order to minimize translational energy in the fragments, this implies that (DF)₂ requires higher j states in the predissociating flux to absorb the excess vibrational energy. To couple such higher j states in the dissociation event requires higher order anisotropy in the potential, which could therefore account for the slowing of the predissociation rate upon D/H substitution.

At a more quantitative level, however, this interpretation breaks down. After one subtracts the different dissociation energies for (HF)₂ and (DF)₂, energetically near resonant product channels for vibrational predissociation of the two isotopomers prove to have comparable final j states. For example, the nearest

channel for ν_1 excitation of HF dimer is $j_1 = 10$ and $j_2 = 5$ (with $\Delta E \approx 18 \text{ cm}^{-1}$ excess energy for $J = 0$), while for DF dimer it is $j_1 = 10$ and $j_2 = 7$ (with $\Delta E \approx 0 \text{ cm}^{-1}$ excess energy for $J = 0$). This reflects only a rather modest difference ($\Delta j_2 = 2$) in the final j state distribution, and in the less rotationally excited species. In other cluster systems, the isotopic dependence could be due to a near resonant V-V channel, resulting in formation of a vibrationally excited fragment that exists for one isotopomer, but is “detuned” for the other, such as was observed in the isotopically substituted pairs H₂-HF/D₂-HF and N₂-HF/N₂-DF.^{66,67} In the *unmixed* HF-HF and DF-DF dimers, however, the dissociation energies eliminate any possibility of vibrationally excited product channels. Additionally, from explicit state counts of asymptotic rotational levels, there is no systematic difference between the nature of channels open in (DF)₂ vs. (HF)₂ predissociation events. Indeed, if anything there is a *higher* density of final states open to (DF)₂ predissociation, which from a statistical perspective would tend to enhance rather than diminish the predissociation rates. Finally, if isolated energetic near resonances were playing a dominant role in influencing the predissociation rates, some J dependence might be expected, which is in fact not observed for ν_1/ν_2 excitation in either (HF)₂ or (DF)₂.

It is worth stating, however, that such a strong J dependence on vibrational predissociation rate is clearly evident in slit jet studies of the *mixed* HF-DF and DF-HF dimers,⁵¹ which does provide direct evidence for vibrational states “tuning” in and out of resonance with increasing rotational excitation. Interestingly, this resonance phenomenon occurs *only* when the mixed dimer is

excited in the HF moiety, whereas the spectra are quite unperturbed for rotational levels built on the fundamental DF stretch excitation. As discussed elsewhere,⁵¹ this arises from intermolecular V - V transfer from the HF($v = 1$) stretch excited states to high intermolecular combination states built on the DF($v = 1$) excited species. The lack of any J dependent perturbations in the DF stretch excited spectra is easily explained in this model, since the inverse process is energetically closed. Thus, the signature of unimolecular resonance phenomena in these predissociation lineshapes is typically quite clear, and not observed in the (DF)₂ ν_1/ν_2 spectra.

As a final note, the mode, isotope and K dependence of these predissociation lifetimes provide a demanding set of tests of trial potential energy surfaces for hydrogen bonding. These lifetimes are quite challenging to calculate theoretically, since it necessarily requires treating both intra and intermolecular degrees of freedom with a comparable level of rigor. Recently, Zhang and coworkers have calculated predissociation rates of selected vibrational states in HF-HF.^{36,40,41} Theoretical advances from Manolopolous and Alexander^{68,69} in time dependent flux treatments have been utilized by Zhang and coworkers to calculate predissociation rates in the mixed dimers HF-DF and DF-HF.⁷⁰ It is therefore clear that the theoretical tools now exist to calculate the corresponding predissociation lifetimes in DF-DF; to date, however, we are aware of no rigorous quantum theoretical calculations of ν_1/ν_2 predissociation rates on trial potential surfaces with which to compare our experimental results. As a further stimulus of such theoretical efforts, we have also recently measured predissociation rates,

vibrational frequencies, tunneling splittings and rotational constants for all four *intermolecular* modes (i.e. “van der Waals stretch”, “geared bend”, “antigeared bend” and “out-of-plane torsion”) in both (HF)₂^{46,48} and (DF)₂⁴⁹ as combination bands built on either ν_1 or ν_2 excitation. In conjunction with full 6-D theoretical analysis, this combined data set should provide considerable spectroscopic leverage for quantitative refinement of potential energy surfaces in this prototypic hydrogen bonded system.

7.5 Summary

A comprehensive study of the high frequency intramolecular ν_1 and ν_2 modes for (DF)₂ is presented, as elucidated via direct absorption near IR spectroscopy in a slit supersonic jet expansion. The rotational progressions for $K = 0$ and $K = 1$ bands of both the “free” and “bound” intramolecular modes have been assigned and analyzed using a near symmetric top energy level expression. The shifts in measured rotational constants have been interpreted in terms of changes in the vibrationally averaged wavefunction, indicating both a contraction and bending of the hydrogen bond upon intramolecular excitation. The tunneling splittings have been presented as a function of isotope, intramolecular vibration, and K rotational excitation. A simple 1-D picture based on semiclassical WKB analysis has been used to account for the different K dependence of tunneling splitting observed in the (HF)₂ and (DF)₂ isotopomers. Finally, high resolution analysis of spectral lineshapes has been used to determine vibrational

predissociation rates in vibrationally excited $(DF)_2$. The system demonstrates a clear mode specific enhancement of predissociation rates upon ν_2 (“bound”) vs. ν_1 (“free”) excitation. This behavior is quite similar to what has been observed in the analogous $(HF)_2$ vibrational levels,¹⁹ but with an overall reduction in predissociation rate upon H/D isotopic substitution. The clear repetition of this mode specific pattern between HF-HF and DF-DF predissociation rates, as well as the absence of any J dependence to the linewidths, provides support for a non-resonant, impulsive description of the predissociation event. The recent significant advances both in the availability of high resolution spectroscopic data, as well as full 6-D quantum theoretical methods for calculating experimentally observable quantities with no dynamical approximations, are beginning to provide new prospects for rigorous testing of trial potential surfaces in all molecular degrees of freedom.

References for Chapter 7

- ¹ Z. S. Huang, K. W. Jucks, and R. E. Miller, *J. Chem. Phys.* **85**, 6905 (1986).
- ² P. A. Block and R. E. Miller, *Chem. Phys. Lett.* **226**, 317 (1994).
- ³ R. L. Deleon and J. S. Muentzer, *J. Chem. Phys.* **80**, 6092 (1984).
- ⁴ A. S. Pine and W. J. Lafferty, *J. Chem. Phys.* **78**, 2154 (1983).
- ⁵ D. J. Nesbitt, *Mode Selective Chemistry, Proceedings 24th Jerusalem Symposium*, 113 (1991).
- ⁶ G. T. Fraser, *Int. Rev. Phys. Chem.* **10**, 189 (1991).
- ⁷ J. G. Loeser, C. A. Schmuttenmaer, R. C. Cohen, M. J. Elrod, D. W. Steyert, R. E. Bumgarner, and G. A. Blake, *J. Chem. Phys.* **97**, 4727 (1992).
- ⁸ M. D. Schuder, C. M. Lovejoy, R. Lascola, and D. J. Nesbitt, *J. Chem. Phys.* **99**, 4346 (1993).
- ⁹ T. R. Dyke, B. J. Howard, and W. Klemperer, *J. Chem. Phys.* **56**, 2442 (1971).
- ¹⁰ B. J. Howard, T. R. Dyke, and W. Klemperer, *J. Chem. Phys.* **81**, 5417 (1984).
- ¹¹ H. S. Gutowsky, C. Chuang, J. D. Keen, T. D. Klots, and T. Emilsson, *J. Chem. Phys.* **83**, 2070 (1985).
- ¹² W. J. Lafferty, R. D. Suenram, and F. J. Lovas, *J. Mol. Spectrosc.* **123**, 434 (1987).
- ¹³ W. Klemperer, *Ber. Bunsenges. Phys. Chem* **78**, 128 (1974).
- ¹⁴ A. S. Pine, W. J. Lafferty, and B. J. Howard, *J. Chem. Phys.* **81**, 2939 (1984).
- ¹⁵ A. S. Pine and B. J. Howard, *J. Chem. Phys.* **84**, 590 (1986).

- 16 A. S. Pine, in *Structure and Dynamics of Weakly bound Molecular Complexes*, edited by A. Weber (D. Reidel Publishing Company, New York, 1987), pp. 93.
- 17 E. J. Bohac, M. D. Marshall, and R. E. Miller, *J. Chem. Phys.* **96**, 6681 (1992).
- 18 E. J. Bohac and R. E. Miller, *J. Chem. Phys.* **99**, 1537 (1993).
- 19 A. S. Pine and G. T. Fraser, *J. Chem. Phys.* **89**, 6636 (1988).
- 20 H.-C. Chang and W. Klemperer, *J. Chem. Phys.* **98**, 9266 (1993).
- 21 H.-C. Chang and W. Klemperer, *J. Chem. Phys.* **100**, 1 (1994).
- 22 M. A. Suhm, J. T. Farrell, Jr., A. McIlroy, and D. J. Nesbitt, *J. Chem. Phys.* **97**, 5341 (1992).
- 23 A. E. Barton and B. J. Howard, *Faraday Discuss. Chem. Soc.* **73**, 45 (1982).
- 24 D. R. Yarkony, S. V. O'Neil, H. F. Schaefer III, C. P. Baskin, and C. F. Bender, *J. Chem. Phys.* **60**, 855 (1974).
- 25 G. C. Hancock, D. G. Truhlar, and C. E. Dykstra, *J. Chem. Phys.* **88**, 1786 (1988).
- 26 M. H. Alexander and A. E. DePristo, *J. Chem. Phys.* **65**, 5009 (1976).
- 27 W. L. Jorgensen, *J. Chem. Phys.* **70**, 5888 (1979).
- 28 P. R. Bunker, M. Kofranek, H. Lischka, and A. Karpfen, *J. Chem. Phys.* **89**, 3002 (1988).
- 29 M. Kofranek, H. Lischka, and A. Karpfen, *J. Chem. Phys.* **121**, 137 (1988).
- 30 D. G. Truhlar, in *Dynamics of Polyatomic Van der Waals Complexes*, edited by N. Halberstadt and K. C. Janda (Plenum Press, New York, 1990), pp. 159.
- 31 M. Quack and M. A. Suhm, *J. Chem. Phys.* **95**, 28 (1991).
- 32 D. H. Zhang, Q. Wu, J. Z. H. Zhang, M. von Dirke, and Z. Bacic, *J. Chem. Phys.* **102**, 2315 (1995).

- 33 W. C. Necochea and D. G. Truhlar, *Chem. Phys. Lett.* **224**, 297 (1994).
- 34 W. C. Necochea and D. G. Truhlar, *Chem. Phys. Lett.* **231**, 125 (1994).
- 35 H. Sun and R. O. Watts, *J. Chem. Phys.* **92**, 603 (1990).
- 36 D. H. Zhang, Q. Wu, J. Z. H. Zhang, M. von Dirke, and Z. Bacic, *J. Chem. Phys.* **102**, 2315 (1995).
- 37 Z. S. Huang, K. W. Jucks, and R. E. Miller, *J. Chem. Phys.* **85**, 3338 (1986).
- 38 M. Quack and M. A. Suhm, *Chem. Phys. Lett.* **234**, 71 (1995).
- 39 N. Halberstadt, P. Brechignac, J. A. Beswick, and M. Shapiro, *J. Chem. Phys.* **84**, 170 (1986).
- 40 D. H. Zhang and J. Z. H. Zhang, *J. Chem. Phys.* **99**, 6624 (1993).
- 41 D. H. Zhang and J. Z. H. Zhang, *J. Chem. Phys.* **98**, 5978 (1993).
- 42 E. Riedle, S. H. Ashworth, J. T. Farrell, Jr., and D. J. Nesbitt, *Rev. Sci. Instrum.* **65**, 42 (1994).
- 43 J. T. Farrell, Jr., S. Davis, and D. J. Nesbitt, *J. Chem. Phys.* **103**, 2395 (1995).
- 44 A. S. Pine, *J. Opt. Soc. Am.* **64**, 1683 (1974).
- 45 R. S. Ram, Z. Morbi, B. Guo, K. Q. Zhang, P. F. Bernath, J. V. Auwera, J. W. C. Johns, and S. P. Davis (unpublished data)
- 46 D. T. Anderson, S. Davis, and D. J. Nesbitt, *J. Chem. Phys.* **104**, 6225 (1996).
- 47 I. M. Mills, *J. Chem. Phys.* **88**, 532 (1984).
- 48 D. T. Anderson, S. Davis, and D. J. Nesbitt, *J. Chem. Phys.* **105**, 4488 (1996)
- 49 S. Davis, D. T. Anderson, and D. J. Nesbitt, *J. Chem. Phys.* **105**, 6645 (1996)
- 50 J. T. Hougen and N. Ohashi, *J. Mol. Spectrosc.* **109**, 134 (1985).

- 51 J. T. Farrell, Jr., M. A. Suhm, and D. J. Nesbitt, *J. Chem. Phys.* **104**, 9313 (1996)
- 52 M. D. Schuder, D. D. Nelson, Jr., and D. J. Nesbitt, *J. Chem. Phys.* **99**, 5045 (1993).
- 53 E. L. Silbert III, *J. Chem. Phys.* **93**, 5022 (1989).
- 54 G. C. Hancock and D. G. Truhlar, *J. Chem. Phys.* **90**, 3498 (1989).
- 55 P. R. Bunker, T. Carrington, Jr., P. C. Gomez, M. D. Marshall, M. Kofranek, H. Lischka, and A. Karpen, *J. Chem. Phys.* **91**, 5154 (1989).
- 56 M. D. Marshall, P. Jensen, and P. R. Bunker, *Chem. Phys. Lett.* **176**, 255 (1991).
- 57 S. C. Althorpe, D. C. Clary, and P. R. Bunker, *Chem. Phys. Lett.* **187**, 345 (1991).
- 58 M. Quack and M. A. Suhm, *Chem. Phys. Lett.* **183**, 187 (1991).
- 59 G. T. Fraser, *J. Chem. Phys.* **90**, 2097 (1989).
- 60 H. C. Chang and W. Klemperer, *J. Chem. Phys.* **104**, 7830 (1996)
- 61 C. H. Townes and A. L. Schawlow, *Microwave Spectroscopy* (Dover Publications, New York, 1975).
- 62 J. M. Lisy, A. Tramer, M. F. Vernon, and Y. T. Lee, *J. Chem. Phys.* **75**, 4733 (1981).
- 63 K. von Puttkamer and M. Quack, *Chem. Phys.* **139**, 31 (1989).
- 64 S. Davis, J. T. Farrell, Jr., D. T. Anderson, and D. J. Nesbitt, *Chem. Phys. Lett.* **246**, 157 (1995)
- 65 G. E. Ewing, *J. Phys. Chem.* **91**, 4662 (1987).
- 66 D. J. Nesbitt, T. G. Lindeman, J. T. Farrell, Jr., and C. M. Lovejoy, *J. Chem. Phys.* **100**, 775 (1994).
- 67 C. M. Lovejoy, D. D. J. Nelson, and D. J. Nesbitt, *J. Chem. Phys.* **89**, 7180 (1988).

- ⁶⁸ M. H. Alexander and D. E. Manolopoulos, *J. Chem. Phys.* **97**, 4832 (1992).
- ⁶⁹ D. E. Manolopoulos and M. H. Alexander, *J. Chem. Phys.* **97**, 2527 (1992).
- ⁷⁰ D. H. Zhang, Q. Wu, and J. Z. H. Zhang, *J. Chem. Phys.* **102**, 124 (1995).